Exploring the Next-Generation High-Reliability Lead-free Solder Alloy

Pritha Choudhury, Ph.D., Morgana Ribas, Ph.D.,
Prathap Augustine, Siuli Sarkar, Ph.D., Paul Salerno, Anna Lifton
MacDermid Alpha Electronics Solutions
Bangalore, India
Pritha.Choudhury@MacDermidAlpha.com; Paul.Salerno@MacDermidAlpha.com

Lijia Xie, Sean Yenyu Lai, David Neal Halbrook, Ganesh Subbarayan, Ph.D., John Blendell, Ph.D.
Purdue University
West Lafayette
IN, USA
blendell@purdue.edu

ABSTRACT

The ever-increasing demand for high-temperature reliability and extended fatigue life requirements in more demanding electronic applications, has motivated further investigation on high-reliability lead-free solder alloys. The novel Alloy 10 solder alloy presented here exhibits exemplary thermomechanical and mechanical reliability in extreme operating conditions, ideal for the future needs of high-reliability electronics, such as in the automotive industry.

Recent results showing excellent performance of Alloy 10 when compared to another leading high-reliability alloy, have also raised questions on which features are responsible for such performance. In this work, we present the latest results of a collaborative in-depth study to understand the mechanisms behind the Alloy 10 solder alloy's improved performance. Solder joint samples are studied for the detailed composition and distribution of phases after reflow and aging treatment under varying aging times. The effect of aging time and temperature on the evolution of the microstructure of the solder joints is then studied. A redistribution of elements and phases are observed after aging; microconstituents are observed to be uniformly distributed after prolonged aging, while intermetallic compounds grow and become distinctly visible upon aging. This discussion is then further expanded by discussing the mechanical behaviour of Alloy 10 as measured by a custom designed micro-precision mechanical tester, which was used to perform isothermal creep, monotonic and fatigue testing of solder test specimens under shear at room temperature.

Key words: High-reliability, automotive, aging, microstructure.

INTRODUCTION

Alloy compositions and thermal profile are known to affect the microstructure and mechanical properties of lead-free solder joints [1]. The thermomechanical response of SAC solder joints in service depends on the size, number, and distribution of these precipitates such as Ag_3Sn and Cu_6Sn_5. For example, a solder joint with many fine Ag_3Sn precipitates is much stronger than a joint with a few large Ag_3Sn precipitates. In addition, Bi and Sb having high solubility in Sn can result in solid solution strengthening of the solder joint. Considering the rapid miniaturization and the extreme temperature conditions that solder joints are exposed to (particularly automotive applications) makes their reliability of fundamental interest to electronics manufacturing engineers and industries [2, 3]. Thermal changes induced by either environmental variations or power transients, with the resulting mismatch between coefficient of thermal expansion of the various package materials, results in time and temperature dependent creep deformation of solder [2]. The creep deformation accumulates with repeated cycling and ultimately causes solder joint cracking and interconnect failure. Thermal aging of the solder joints could induce changes in the microstructure and could trigger creep failure resulting in reduced joint reliability [2, 3, 4, 5, 6, 7]. Creep being the primary factor contributing tothermomechanical fatigue failure, it is critical to study the microstructural changes and the underlying mechanisms associated with thermal aging. Analyzing the solder joint microstructure plays important role in understanding long-term solder joint behavior. Conditions of temperature, duration of aging and surface finish can be factors that significantly affect the solder joint constitutive behaviour that in turn affects the reliability of solder joints [8, 9].

In response to the above, a detailed investigation into the effect of aging temperature and time on an ultra-high reliability alloy (Alloy 10) developed by MacDermid Alpha to address the current and future needs of the automotive industry is presented here as part of a collaborative study with Purdue University.

EXPERIMENTAL METHODS

The liquidus temperature, solidus temperature, and undercooling are identified by differential scanning calorimetry (DSC) studies. Differential Scanning Calorimetry (DSC) is done at the rate of 10ºC/ minute.

High temperature tensile tests have been done for Alloy 10 at 150°C and compared with that of the standard High Rel Alloy.

Alloy 10, the alloy used in this study, is obtained as 500 µm spheres and made into sandwich samples or bilateral solder joints as shown in Figure 1. The sandwich samples were prepared by hand-placing solder balls and flux onto the BGA test board with the organic surface preservative (OSP) or electroless nickel immersion gold (ENiG) surface finish. Samples were reflowed according to the profile, shown in Figure 2, in a DDM Novastar GF-12HC-HT 3-zone tabletop reflow oven with a peak temperature of 240°C for two times due to the fabrication process. The bottom circuit board and solder balls went into the reflow oven during the first time reflow process, and then the top circuit board was added in the second reflow process. Effectively, the bottom circuit board has undergone two times reflow, while the top circuit board has undergone one time reflow. Next, the sandwich samples were mounted in room-temperature epoxy, cross-sectioned, and polished to a 0.05 µm diamond suspension in a MetPrep 3™ 5-2600 auto-polisher.

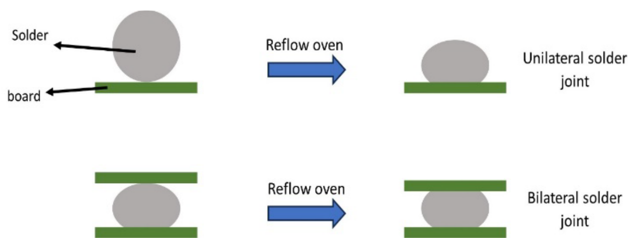

Figure 1. Formation of solder joint samples

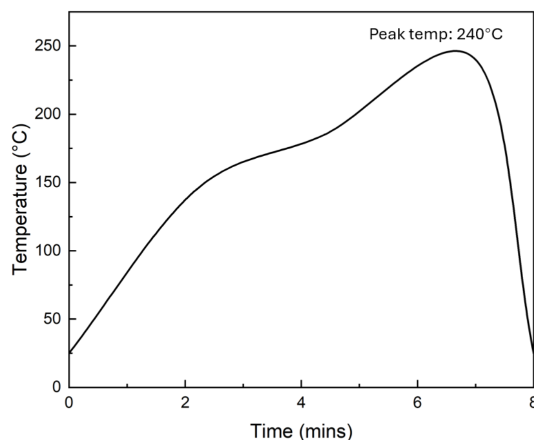

Figure 2. Reflow Profile for Soldering

Samples are aged at 125°C or 150°C for 3, 7, 10, and 15 days in Fisher Scientific Isotemp Oven. The sandwich samples were then mounted in room-temperature epoxy, cross-sectioned, and polished to a 0.05 µm diamond suspension in a MetPrep 3™ 5-2600 auto-polisher.

Scanning electron microscopy (SEM) with the back-scattered electron mode (BSE) is used to identify different phases in the microstructure. Electron dispersive spectroscopy (EDS) is used to verify the composition of different compounds. Fiji-ImageJ is used to analyze microstructure images and calculate the intermetallic compound (IMC) layer thickness.

A closed-loop 'micro-precision tester' custom designed to carry out joint-scale testing of solder joints was used in this study (Figure 3). Joint scale testing as opposed to bulk testing of dog-bone shaped samples, is essential to capture the effect of the solder joints and that of the surface finish. The tester description is given in details in reference [10]. Closed-loop testing ensures that displacement and its rate is measured at the sample eliminating load train compliance that causes sample displacement to deviate from crosshead movement.

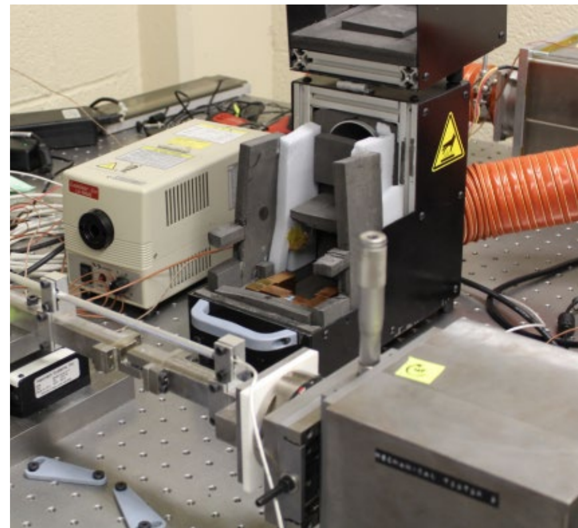

Figure 3. The micro-precision mechanical tester with the environmental chamber.

The solder joints design with a diameter of 730 µm and standoff height of 150 µm is shown in Figure 4. Such low aspect ratio joints ensure a more homogeneous shear stress at the pad interface as described in reference [11]. FR4 substrates which are mask-defined single-layer PCBs with ENiG or OSP finishes are used for the monotonic shear test. Eight solder joints are sandwiched between two such PCBs as shown in Figure 4. Hence, such low aspect ratio squat joints help to produce a more uniform state of stress at the solder-pad interface thereby relating a given applied load to a unique state of stress at the interface.

Alloy 10 was characterized in this study with OSP surface finish on the substrates using strain (0.2 µm/s) controlled monotonic tests. Samples were tested in the as-reflowed condition and after aging at 125°C for 10 days.

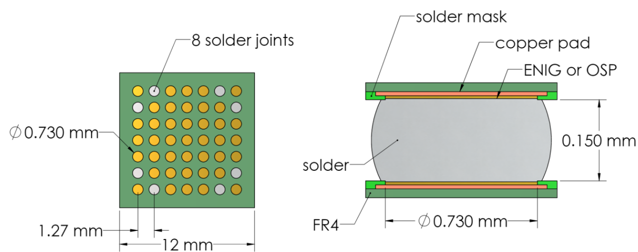

Figure 4. Cross-section of a single solder joint and the substrate used to build sandwich test specimen with solder joint locations as denoted.

The von Mises distortion energy theory is used to approximate the equivalent uniaxial tensile stress σ and engineering strain ϵ within the solder joints as $\sigma = \sqrt{3}Fz/A$ and $\epsilon = \Delta z/\sqrt{3}h$, where, Fz is the applied shear load, A the total pad area, Δz the measured shear displacement and h the standoff height. Accordingly, the equivalent stress corresponding to a force of 50N is 25.9 MPa and the equivalent strain rate in monotonic shear experiments is $7.7\times10^{-4}s^{-1}$.

RESULTS AND DISCUSSION

The alloy used in this study is based on Sn-Ag-Cu, with additions of Bi and Sb. Table 1 highlights a generic description of the alloy. Bi addition is 30 to 50% of the added Sb. Also, this alloy contains alloying additions (generically referred as X) that constitute less than 0.5 wt.% of the alloy composition.

Table 1. Generic description of the alloys

Alloy ID	Generic Description
High Rel Alloy	Sn-Ag-Bi-Sb-Cu-Ni
Alloy 10	Sn-Ag-Bi-Sb-Cu-X

The results of the DSC studies are shown in Figure 5. The standard High Rel Alloy has a large undercooling of ~45ºC while Alloy 10 has an undercooling of only ~11ºC. Large undercooling prior to solidification can produce large grains in the solder joint, anisotropic behaviour and undesirable mechanical properties [12]. The occurrence of small undercooling is expected to result in superior mechanical properties in Alloy 10.

The microstructures of the standard High Rel Alloy and Alloy 10 are shown in Figure 6 (a) and (b), respectively. It is observed that Alloy 10 has finer grain size than the standard High Rel Alloy. The small undercooling in Alloy 10 has resulted in finer grain size that in turn is expected to result in superior mechanical properties.

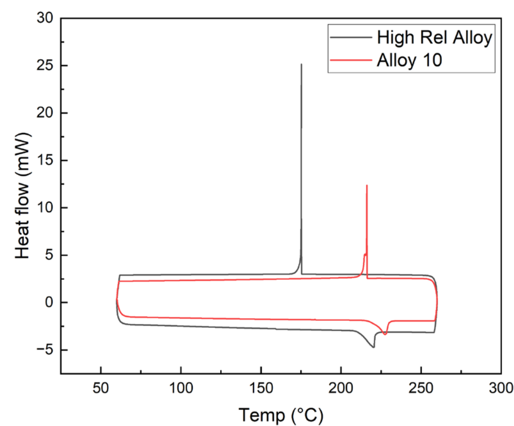

Figure 5. DSC plot of High Rel Alloy and Alloy 10

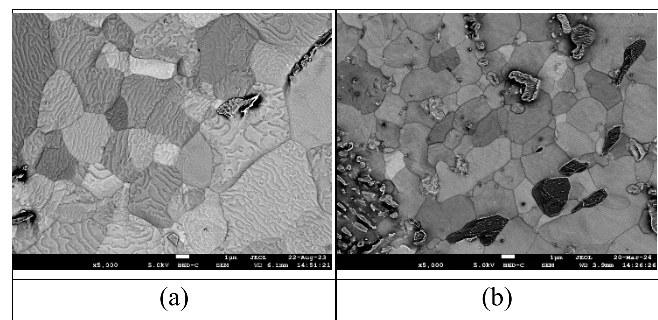

Figure 6. Microstructure of (a) High Rel Alloy and (b) Alloy 10 in As-cast Condition

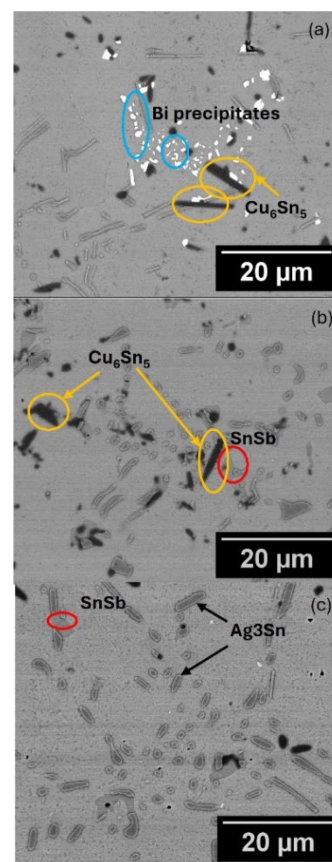

Figure 7. Alloy 10 on Cu OSP (a) as reflowed and aged for 3 days at (b) 125C and (c) 150C.

The microstructure of Alloy 10 under different conditions is shown in Figure 7. Bi precipitates observed in the as reflowed condition dissolves in the Sn phase with aging at either temperature. Similar feature of Bi dissolution is also observed on ENiG surface as shown in Figure 8. However, in this case, the Bi dissolution is complete at 150°C but not at the lower temperature. In both cases, SnSb phase starts precipitating with aging. The SnSb phase appears in two different morphologies, faceted and particle shape. In addition to the usual intermetallic phases, Ag_3Sn and $(Cu,Ni)_6Sn_5$, $AuSn_4$ is observed on the ENiG surface.

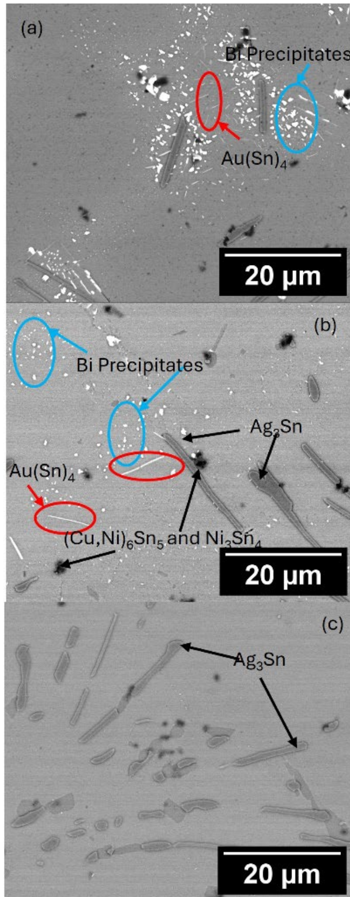

Figure 8. Alloy 10 on ENiG (a) as reflowed and aged for 3 days at (b) 125°C and (c) 150°C.

An overall comparison of the Alloy 10 across the total period of aging on Cu OSP surface is shown in Figure 9. Bi that dissolves after 3 days aging reprecipitates after 10 days of aging and then again dissolve in Sn phase at 15 days aging. SnSb particles appear after 3 days and grow with increasing aging time.

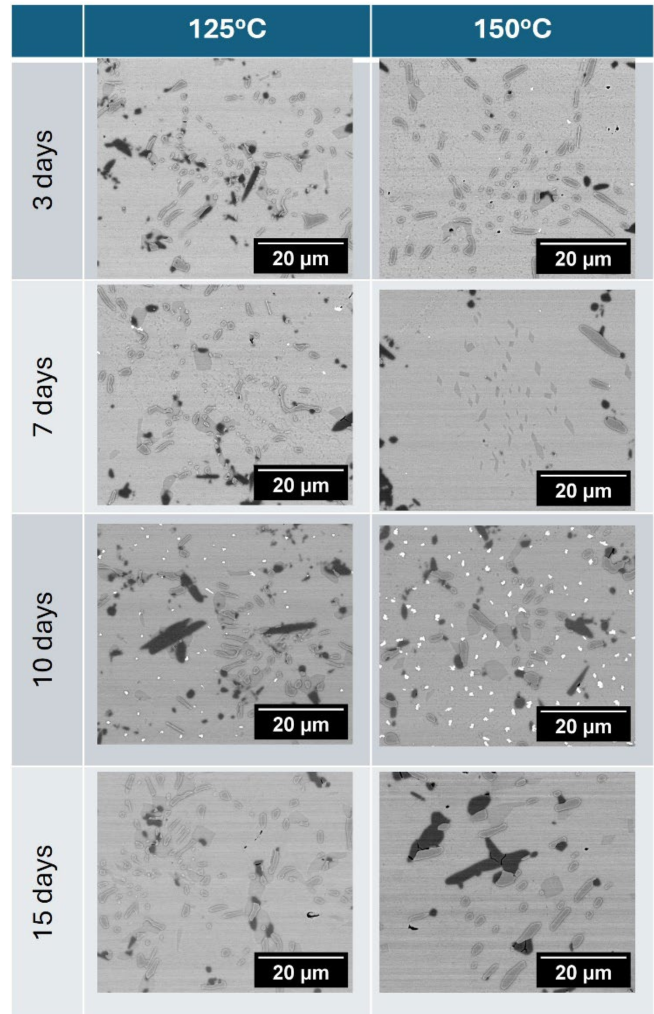

Figure 9. Evolution of Alloy 10 on Cu OSP microstructure during aging up to 15 days.

The change in the interfacial IMC thickness with aging time at different temperatures on OSP surface is shown in Figure 10, for the single and double reflow sides, respectively. Aging at higher temperature is associated with greater diffusion of atoms and thereby results in thicker interfacial IMC layer. Additionally, Cu_3Sn layer starts forming after 3 days of aging at 150°C and grows at a significantly higher rate at this temperature. The double reflow side interface being exposed to reflow conditions for longer time, has an IMC of greater initial and final thickness as shown in Figure 10 (b).

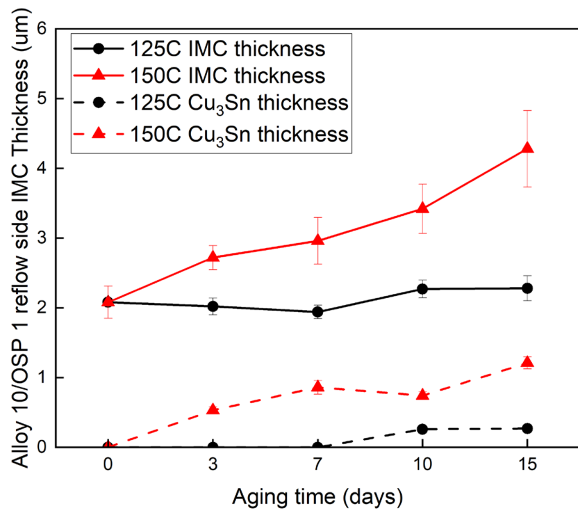

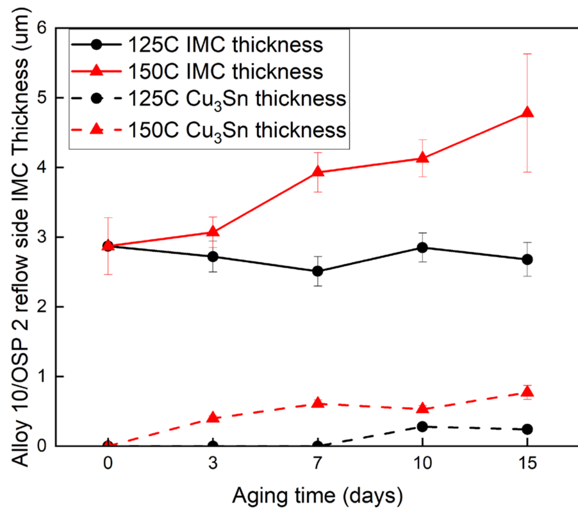

Figure 10. Change in IMC thickness on OSP surface on single reflow and double reflow side.

An overall comparison of the Alloy 10 across the total period of aging on ENiG surface is shown in Figure 11. Similar changes in dissolution and reprecipitation of Bi as on OSP surface is observed here too.

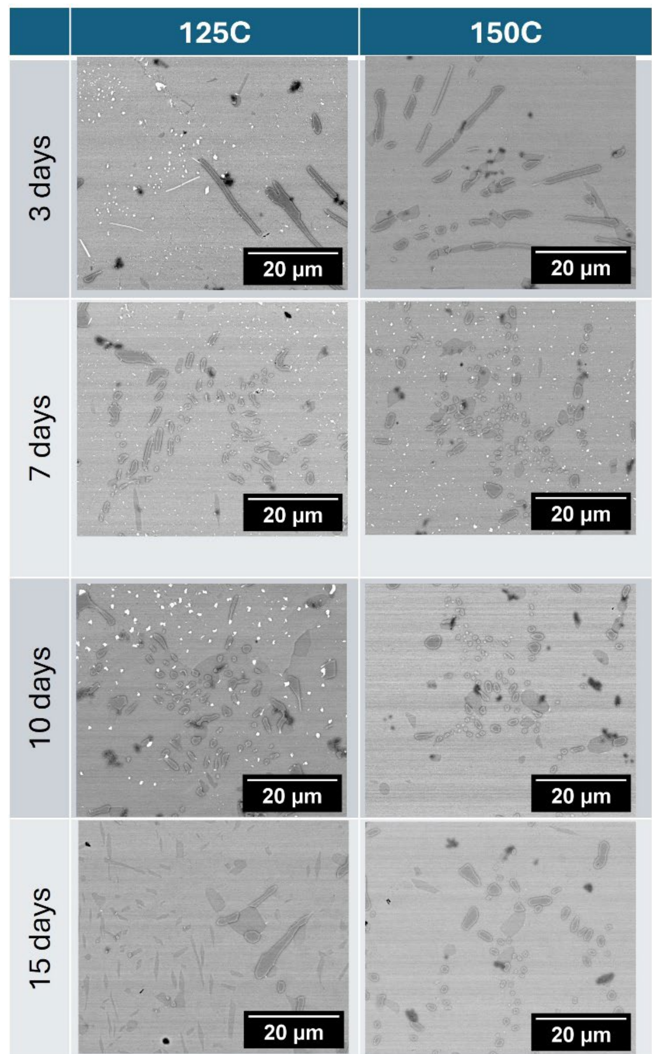

Figure 11. Evolution of Alloy 10 on ENiG microstructure during aging up to 15 days.

The change in the interfacial IMC thickness with time on ENiG surface is shown in Figures 12 (a) and (b), for the single and double reflow sides, respectively. Similar trend of higher initial thickness in double reflow and higher temperature of aging is observed. The diffusion barrier created by the ENiG surface leads to minimal growth of IMC at either temperature compared to OSP surface and resists the formation of Cu_3Sn layer even till 15 days' aging.

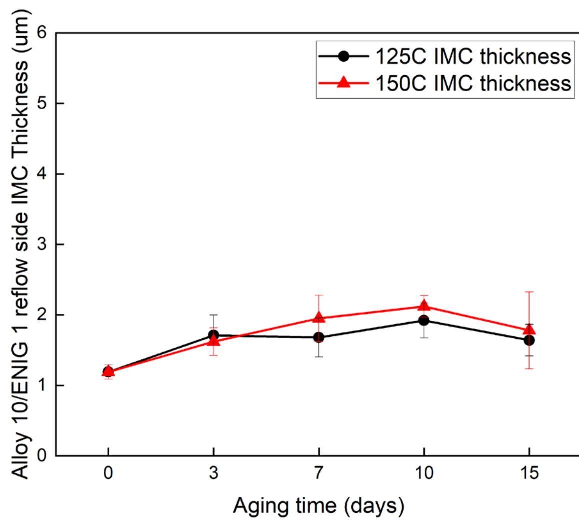

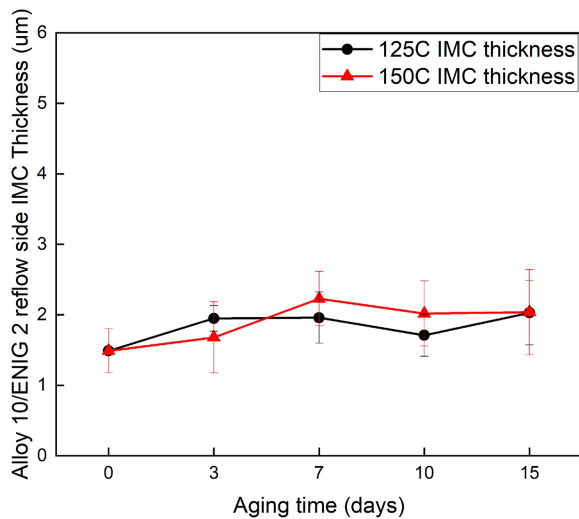

Figure 12. Change in IMC thickness on ENiG surface on single reflow and double reflow side.

The results of the monotonic shear test are shown in Figure 13. The Alloy 10 solder joint maintains nearly the same strength before and after aging. The precipitation of SnSb and the dissolution of Bi (resulting in solid solution strengthening) after aging helps to retain its strength for a longer time post-aging.

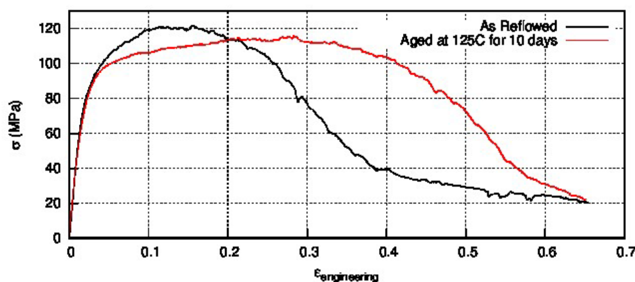

Figure 13. Results of Monotonic Shear Test of Alloy 10

The cross-sections of the solder joints after monotonic shear test are shown in Figure 14.

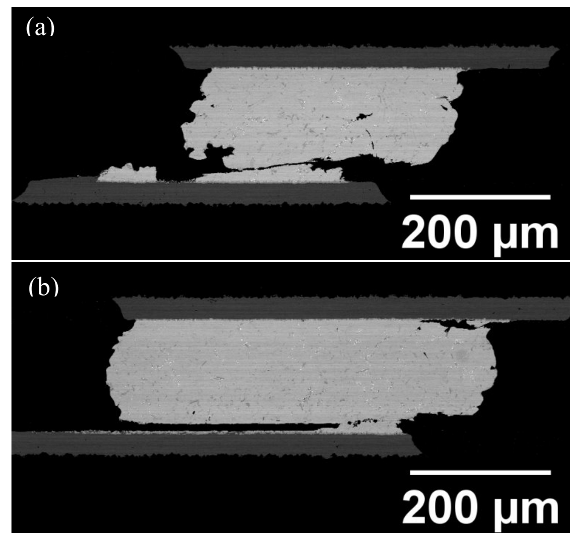

Figure 14. Alloy 10 (as reflowed) Solder Joint after Monotonic Shear Test

In Figures 14(a) and (b), the crack initiates in the interfacial IMC and then propagates through the bulk. Thus, both interfacial and bulk solder joint failures are observed in the as-reflowed solder joint after monotonic shear test.

The results of the high temperature tensile tests and thermal cycling (air-air) are shown in Figures 15 and 16, respectively. Thermal cycling was done at -40ºC to 150ºC, with 30 minutes dwell at each temperature, up to 2500 cycles. The electrical resistance failures are plotted using Weibull plot.

Both alloys exhibit nearly equal strength but Alloy 10 is able to sustain a longer elongation before failure. Such a behaviour will enable the alloy to accommodate stresses generated during thermal cycling, resulting in longer survival of the solder joints. The alloy is expected to be more resistant to harsh environment thermal cycling condition as shown in Figure 16. The characteristic life of Alloy 10 is more than 40% higher than that of the High Rel Alloy.

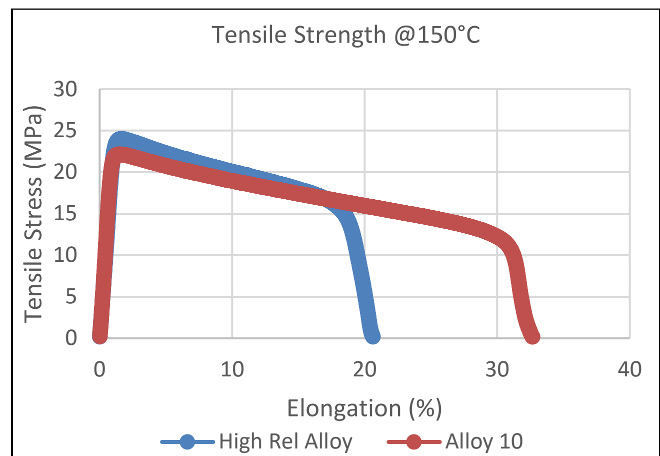

Figure 15. High temperature tensile properties

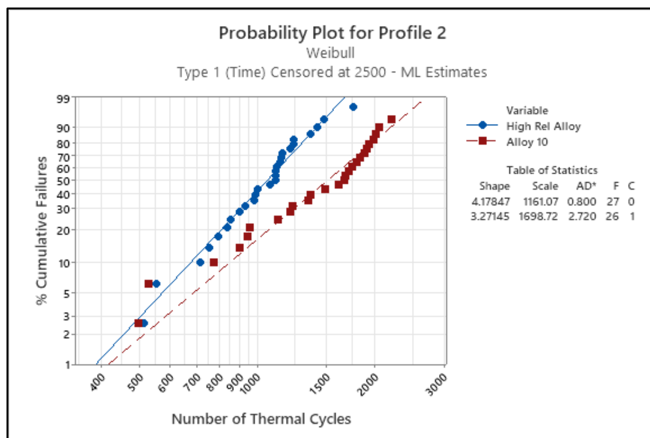

Figure 16. Weibull plot for thermal cycling at -40°C to 150°C, 30 minutes dwell time

CONCLUSIONS

Increase in complex electronic assemblies exposed to harsh environmental conditions has motivated the need for advancement of solder alloy technology. Migration of automotive industry to electric vehicles and autonomous driving that require extended service life in harsh operating conditions is the driving force for the adoption of high reliability solder alloys. The new high reliability Alloy 10 developed at MacDermid Alpha has been studied in detail to understand the mechanism behind its improved performance.

Key conclusions are:

- Very low undercooling of ~11°C is observed in Alloy 10 compared to a high undercooling of ~45°C in the standard High Rel Alloy has resulted in finer grain size in Alloy 10. The dissolution of Bi and precipitation of SnSb particles helps maintain the high strength of Alloy 10 for a longer time after aging.
- Higher elongation of Alloy 10 during high temperature tensile test indicates a better performance when subjected to thermal cycling in extreme temperature conditions.
- Alloy 10 is also observed to have much higher characteristic life than the High Rel Alloy during thermal cycling.

Work is ongoing on further mechanical and thermomechanical properties evaluation of the Alloy 10 solder joints and the failure analysis to understand the underlying mechanisms.

REFERENCES

[1] Wang S., et al., "Critical Review of Size Effects on Microstructure and Mechanical Properties of Solder Joints for Electronic Packaging", *Appl. Sci.,* vol. 9 (2019) 1-15.

[2] Depriver Joshua A., et al., "Creep Damage of BGA Solder Interconnects Subjected to Thermal Cycling and Isothermal Aging", *Proc. Of 21st Electronics Packaging Technology Conference*, (2019).

[3] Depriver J., et al., "Solder Joint Failures Under Thermo-mechanical Loading Conditions – A Review", *University of Derby.*

[4] Ma Hongtao et al., "Reliability of Lead-free Solder Joints Under a Wide Range of Thermal Cycling Conditions", *IEEE Trans. On Components, Packaging and Manufacturing Technology*, vol. 1 (2011).

[5] Akkara J. F., et al., "Reliability of New SAC-Bi Solder Alloys in Thermal Cycling with Aging", *Proc. Of the SMTA*

[6] Zhang Y., et al., "The Effects of Aging Temperature on SAC Solder Joint Material Behavior and Reliability", *Proc. Of Electronics Components and Technology Conference* (2008) 99-112.

[7] Ronnie Teo J. W., "Thermal Cycling Aging Effect on the Reliability and Morphological Evolution of SnAgCu Solder Joints", *IEEE Trans. On Electronics Packaging Manufacturing,* vol. 30 (2007) 279-284.

[8] Pietrikova A. and Durisin J., "Microstructure of Solder Joints and Isothermal Aging", *Acta Electrotechnica et Informatica*, vol. 10 (2010) 43-46.

[9] Liang J. et al., "Solidification Condition Effects on Microstructures and Creep Resistance of Sn-3.8Ag-0.7Cu Lead-free Solder", *Metallurgical and Materials Trans. A,* vol. 38A (2007) 1530-1538.

[10] P L, Sukshitha Achar, et al. "Comparative Mechanical Behavior of Sn-Bi based Low Temperature Solder Alloys under Different Pretest Aging Conditions." *2023 IEEE 73rd Electronic Components and Technology Conference (ECTC)* (pp. 2218-2222) 2023.

[11] Bhate, D., Chan, D., Subbarayan, G., Chiu, T. C., Gupta, V., & Edwards, D. R. "Constitutive behavior of Sn3. 8Ag0. 7Cu and Sn1. 0Ag0. 5Cu alloys at Creep and Low Strain Rate Regimes". *IEEE Transactions on Components and Packaging Technologies*, vol. 31(2008), 622-633.

[12] Elmer J. W., et al., "Microstructure and In-situ Observations of Undercooling for Nucleation of β-Sn Relevant to Lead-free Solder Alloys", *J. of Electronic Materials*, vol. 39 (2010) 273-282.